

1 **Unusual stratospheric ozone anomalies observed in 22 years**  
2 **of measurements from Lauder, New Zealand**

3 Gerald E. Nedoluha<sup>1</sup>, Ian S. Boyd<sup>2</sup>, Alan Parrish<sup>3</sup>, R. Michael Gomez<sup>1</sup>, Douglas R. Allen<sup>1</sup>,  
4 Lucien Froidevaux<sup>4</sup>, Brian J. Connor<sup>2</sup>, and Richard R. Querel<sup>5</sup>

5 <sup>1</sup>Naval Research Laboratory, Remote Sensing Division, Washington, D. C., USA

6 <sup>2</sup>BC Scientific Consulting LLC, USA

7 <sup>3</sup>Department of Astronomy, University of Massachusetts, Amherst, MA, USA

8 <sup>4</sup>Jet Propulsion Laboratory, California Institute of Technology, Pasadena, California, USA

9 <sup>5</sup>National Institute of Water and Atmospheric Research, Lauder, New Zealand

10 **Abstract**

11 The Microwave Ozone Profiling Instrument (MOPI1) has provided ozone ( $O_3$ ) profiles  
12 for the Network for the Detection of Atmospheric Composition Change (NDACC) at Lauder,  
13 New Zealand ( $45.0^{\circ}S$ ,  $169.7^{\circ}E$ ), since 1992. We present the entire 22 year dataset and compare  
14 with satellite  $O_3$  observations. We study in detail two particularly interesting variations in  $O_3$ .

15 The first is a large positive  $O_3$  anomaly that occurs in the mid-stratosphere ( $\sim 10-30$  hPa) in June  
16 2001, which is caused by an anticyclonic circulation that persists for several weeks over Lauder.

17 This  $O_3$  anomaly is associated with the most equatorward June average tracer equivalent latitude  
18 (TrEL) over the 36-year period (1979-2014) for which the Modern Era Retrospective-Analysis

19 for Research and Applications (MERRA) reanalysis is available. A second, longer-lived feature,  
20 is a positive  $O_3$  anomaly in the mid-stratosphere ( $\sim 10$  hPa) from mid-2009 until mid-2013.

21 Coincident measurements from the Aura Microwave Limb Sounder (MLS) show that these high  
22  $O_3$  mixing ratios are well correlated with high nitrous oxide ( $N_2O$ ) mixing ratios. This  
23 correlation suggests that the high  $O_3$  over this 4-year period is driven by unusual dynamics. The  
24 beginning of the high  $O_3$  and high  $N_2O$  period at Lauder (and throughout this latitude band)

- 1 occurs nearly simultaneously with a sharp decrease in O<sub>3</sub> and N<sub>2</sub>O at the equator, and the period
- 2 ends nearly simultaneously with a sharp increase in O<sub>3</sub> and N<sub>2</sub>O at the equator.

3

4 **1. Introduction**

5 Observations of total column ozone (O<sub>3</sub>) show that, over most of the globe, O<sub>3</sub> loss has  
6 leveled off since ~2000, and O<sub>3</sub> has even begun to increase. The large decline observed from the  
7 1960s to the late 1990s has ended as a result of the reduction in chlorofluorocarbon (CFC)  
8 emissions following the 1987 Montreal Protocol (WMO, 2014). While global O<sub>3</sub> may be  
9 recovering, the magnitude and sign of stratospheric O<sub>3</sub> trends over multi-decadal timescales in  
10 the mid-stratosphere strongly depends on geographical location. It is important to understand the  
11 causes of this geographical variation.

12 Several studies of satellite data show the variability in O<sub>3</sub> trends depending upon the  
13 exact timeframe and geographical location. Kyrölä et al. (2013), using measurements from the  
14 Stratospheric Aerosol and Gas Experiment (SAGE) from 1984-1997, show a general decrease in  
15 O<sub>3</sub> that is statistically significant over much of the stratosphere and is particularly large in the  
16 mid-latitude upper stratosphere. However, they also show an increase in equatorial O<sub>3</sub> (albeit not  
17 statistically significant) in the 30-35 km region.

18 There are a number of studies covering later years, all of which show a variation in O<sub>3</sub>  
19 that differs dramatically from that of the 1984-1997 SAGE data. Nedoluha et al. (2015) studied  
20 O<sub>3</sub> over the period 1991-2005, when Halogen Occultation Experiment (HALOE) measurements  
21 are available, and found a strong decrease in mid-stratospheric O<sub>3</sub> in the tropics over this period.  
22 Kyrölä et al. (2013) also examined the period 1997-2011, showing a general increase in O<sub>3</sub> from  
23 SAGE and Global Ozone Monitoring by Occultation of Stars (GOMOS) measurements, but a

1 statistically significant decrease near 30 km in the tropics. Measurements from the Scanning  
2 Imaging Absorption Spectrometer for Atmospheric Chartography (SCHIAMACHY) instrument  
3 for the period 2002-2012, reported by Gebhardt et al. (2014), showed a pattern similar to the  
4 1997-2011 pattern reported by Kyrölä et al. (2013), i.e., a strong statistically significant decrease  
5 in tropical O<sub>3</sub> in the 30-35 km region while most of the middle atmosphere shows a slight  
6 increase in O<sub>3</sub>. Eckert et al. (2014), using Michelson Interferometer for Passive Atmospheric  
7 Sounding (MIPAS) data from 2002-2012, also showed a general increase in O<sub>3</sub> in most regions,  
8 especially in the Southern Hemisphere mid-latitudes near ~20 hPa, but found statistically  
9 significant negative trends in the tropics from ~25 hPa to 5 hPa. Finally, Nedoluha et al. (2015)  
10 showed that from 2004-2013 Aura MLS measurements showed a strong decrease in mid-  
11 stratospheric O<sub>3</sub> in the tropics. Nedoluha et al. (2015) also showed, based on changes in N<sub>2</sub>O  
12 measured by MLS and NO<sub>x</sub> measured by HALOE, that the decadal scale changes in equatorial  
13 O<sub>3</sub> of the magnitude observed could best be understood as being caused by dynamical variations.  
14 The goal of this paper is to better understand how variations in mid-stratospheric O<sub>3</sub> over Lauder  
15 are affected by large scale dynamical variations, and in particular how air with unusually tropical  
16 characteristics affects the O<sub>3</sub> mixing ratios over Lauder. We will examine in detail two particular  
17 variations in O<sub>3</sub>: a monthly anomaly in 2001 and a 4 year anomaly from 2009-2013. The 4 year  
18 anomaly, when analyzed from the beginning of the Aura MLS time series, results in a positive  
19 linear O<sub>3</sub> trend in the mid-stratosphere over Lauder, in the opposite sense to the trend over this  
20 time period in the tropics. An improved understanding of how dynamical variations affect mid-  
21 stratospheric O<sub>3</sub> variations at this Southern mid-latitude site is important for interpreting  
22 measurements from mid-latitude sites in terms of long-term global O<sub>3</sub> change.

1 This paper is organized as follows. Section 2 describes the ground-based and satellite  
2 measurements. Section 3 examines the MOPI O<sub>3</sub> time series, focusing on the unusual anomalies  
3 in 2001 and 2009-2013. Section 4 examines MOPI O<sub>3</sub> in the context of global O<sub>3</sub> and N<sub>2</sub>O  
4 variations, and a discussion is presented in Section 5.

5

## 6 **2. Measurements**

7 The Microwave Ozone Profiling Instrument (MOPI1) instrument has been making  
8 measurements of stratospheric O<sub>3</sub> from the Network for the Detection of Atmospheric  
9 Composition Change (NDACC) station at Lauder, New Zealand (45.0°S, 169.7°E) since 1992.  
10 With the exception of repairs, the instrument has been essentially unchanged during this entire  
11 period. Both this MOPI1 instrument and the similar MOPI2 instrument deployed at Mauna Loa,  
12 Hawaii, since 1995, have been used as a ground-based reference for a number of satellite  
13 instruments. Satellite measurements can provide a global perspective for the MOPI  
14 measurements, and we will use measurements from Aura MLS to provide such a global  
15 perspective for MOPI ozone variations since 2004. Here we present a brief description of both  
16 the ground-based microwave and satellite measurement techniques.

17

### 18 **2.1 Ground-based microwave measurements**

19 Each MOPI instrument uses a heterodyne receiver coupled to a 120 channel filter  
20 spectrometer to measure the line emission spectrum produced by a thermally excited, purely  
21 rotational ozone transition at 110.836 GHz (2.7 mm wavelength). The spectral intensities and  
22 measurements of the tropospheric thermal emission are calibrated with black body sources at  
23 ambient and liquid nitrogen temperatures. The tropospheric opacity is calculated from hourly

1 emission measurements. The experimental technique was described in Parrish et al. (1992), and  
2 technical details on the instrument used for this work are given in Parrish (1994). MOPI  
3 measurements have been employed in several validation and trend studies (e.g., Boyd et al.,  
4 2007; Steinbrecht et al., 2009).

5 MOPI observations are made continuously, with selected spectra chosen based on the  
6 absolute tropospheric opacity and its variability, where limits for these values are set empirically  
7 at each site. This technique allows measurements in weather ranging from clear sky to some  
8 overcast conditions. The standard MOPI retrieval product, which will be used here, provides  
9 four retrievals per day, using up to 6-hour data periods starting at local midnight. The diurnal  
10 variations in the O<sub>3</sub> measurements from the MOPI2 instrument at Mauna Loa (using a 1-hour  
11 retrieval product) have been validated and compared to the Goddard Earth Observing System  
12 Chemistry Climate Model (GEOSCCM) O<sub>3</sub> (Parrish et al., 2014), and measurements and model  
13 values generally agree to better than 1.5% of the midnight value. For this study we make use of  
14 three of the four daily retrievals, and do not include the daytime afternoon measurements (i.e.,  
15 1200-1800 local time). This selection has been made because, at Lauder, these measurements  
16 show a slightly anomalous vertical profile in the mid-stratosphere, with values at 10 hPa lower  
17 by ~3% than at other times of the day. We believe that these variations may be caused by the  
18 strong thermal cycles in the building housing the instrument, especially in the afternoon.

19 In Fig. 1 we show a typical spectrum and O<sub>3</sub> profile retrieval from the MOPI1 instrument.  
20 As described in Parrish et al. (1992), the measurement shown is obtained using a switching  
21 technique (Parrish et al., 1988) so that the spectrum used in the retrievals is the difference  
22 between measurements being made at a low elevation angle (in this case 22.6° above the  
23 horizon), and measurements made near the zenith through an attenuating sheet of plexiglass.

1 The measured temperature in the two positions is approximately balanced, and any remaining  
2 slope or offset in this difference spectrum is removed before retrieving the O<sub>3</sub> profile. The O<sub>3</sub>  
3 mixing ratio profiles are retrieved from the spectra using an adaptation of the optimal estimation  
4 method of Rodgers (1976), discussed in Parrish et al. (1992) and Connor et al. (1995). Error  
5 analysis techniques are discussed in the latter paper. The independent variable in the retrieval  
6 system is pressure.

7 In Fig. 2 we show typical averaging kernels for the MOPI1 version 6 retrievals. The  
8 vertical resolution of the MOPI1 measurements is ~7-8 km (FWHM) at 10 hPa, slightly coarser  
9 than at Mauna Loa, where the MOPI2 resolution at the 10 hPa pressure level is ~6 km. The  
10 MOPI retrievals have a measurement contribution of near 100% at 10 hPa, as defined by the  
11 technique of Connor et al. (1995). Unless otherwise indicated the satellite measurements which  
12 will be shown have not been convolved with the MOPI averaging kernels.

13

## 14 **2.2 Satellite measurements**

15 We compare MOPI O<sub>3</sub> measurements with observations from three satellites that provide  
16 coincident measurements. Two of these are solar occultation instruments, which make ~15  
17 sunrise and ~15 sunset high vertical resolution (~1 km) profile measurements each day, generally  
18 at different latitudes, with the latitude bands varying differently over the course of the season  
19 depending on the satellite orbit. The majority of MOPI-satellite comparisons come from Aura  
20 MLS, which provides measurements over all latitudes between 82°S and 82°N on a daily basis.

21 The SAGE II instrument was launched in October 1984 aboard the Earth Radiation  
22 Budget Satellite, and continued making measurements through August 2005. It consisted of a  
23 seven channel solar photometer using ultraviolet and visible channels between 0.38 and 1.0  $\mu\text{m}$

1 in solar occultation mode to retrieve atmospheric profiles of ozone, water vapor, nitrogen dioxide  
2 and aerosol extinction. Measurements were made over a latitude range from 80°S to 80°N. The  
3 measurements are retrieved as ozone number density as a function of altitude, but are also  
4 provided as ozone mixing ratio as a function of pressure. The version 6.1 data is described in  
5 Wang et al. (2002).

6 The v7.00 dataset (Damadeo et al., 2013), released in December 2012, is used in this  
7 analysis. This latest processing version implements an algorithm that is consistent across all  
8 SAGE missions. The most significant change in the new version is that, whereas the previous  
9 SAGE retrievals made use of the meteorological profiles from the Climate Prediction Center  
10 (CPC) NCEP analysis, the new retrievals make use of the Modern Era Retrospective-Analysis  
11 for Research and Applications (MERRA) reanalysis. Retrievals using the meteorological  
12 profiles from the MERRA reanalysis show significantly different O<sub>3</sub> mixing ratios as a function  
13 of pressure in the upper stratosphere and mesosphere (pressures below ~4 hPa). For the pressure  
14 levels of interest for this study, however, the differences between the v6.1 and v7.00 SAGE O<sub>3</sub>  
15 retrievals are insignificant.

16 HALOE solar occultation measurements of O<sub>3</sub> are available from 1991-2005. The  
17 latitude bands drifted daily so that near global latitudinal coverage was provided in both sunrise  
18 and sunset modes five times over the course of a year. The trends in the HALOE O<sub>3</sub>  
19 measurements have been compared against SAGE II (Nazaryan et al., 2005) and differences  
20 have been found to be on the order of less than 0.3% per year in a majority of latitude bands at  
21 25, 35, 45, and 55 km.

22 Aura MLS measurements of O<sub>3</sub> and N<sub>2</sub>O are available since 2004. The stratospheric O<sub>3</sub>  
23 product has been validated by Froidevaux et al. (2008). The vertical resolution of the MLS O<sub>3</sub>

1 measurements at 10 hPa is  $\sim$ 3 km. The N<sub>2</sub>O measurements have been validated by Lambert et  
2 al. (2007) and have a vertical resolution of  $\sim$ 4 km. Upper Atmosphere Research Satellite  
3 (UARS) MLS measurements of O<sub>3</sub> are available from 1991-1999, and were validated by  
4 Froidevaux et al. (1996) for the v2.2 retrievals and by Livesey et al. (2003) for the v5 retrievals.

5

### 6 **3. The MOPI O<sub>3</sub> timeseries**

7 In Fig. 3 we show the monthly anomalies at selected pressure levels for the entire  
8 MOPI1 data record. The anomalies are calculated by first fitting the data with a sinusoidal  
9 seasonal cycle (including annual and semi-annual terms) and then subtracting this seasonal cycle  
10 from the data. There are two interesting features that particularly stand out. The first is the large  
11 positive anomaly that occurs in June 2001 at 31.6, 17.7, and 10.0 hPa (green boxes). The  
12 second, much longer-term feature, is the positive anomaly at 10.0 and 5.6 hPa from August 2009  
13 through July 2013 (red boxes). During this period the mean monthly O<sub>3</sub> anomaly at 10 hPa is  
14 0.32 ppmv, only 7 of the 47 measurement months show a negative anomaly, and the 3-month  
15 smoothing never shows a negative anomaly. This period ends with a sharp drop in O<sub>3</sub> in August  
16 2013.

17

#### 18 **3.1 Unusually high mid-stratospheric O<sub>3</sub> in June 2001**

19 Since there are no MLS measurements available to document the global variation in O<sub>3</sub>  
20 during June 2001, we use Tracer Equivalent Latitude (TrEL) simulations in order to better  
21 understand the June 2001 anomaly over Lauder. TrEL is determined from isentropic passive  
22 tracer advection calculations on the sphere as described by Allen and Nakamura (2003). The  
23 tracer mixing ratio is converted to an equivalent latitude by matching the area enclosed by tracer

1 contours to that enclosed by an equivalent latitude line. Specific details of the TrEL calculation  
2 used for this paper, based on MERRA winds, are provided by Allen et al. (2012). The average  
3 TrEL in June 2001 over Lauder on potential temperatures surfaces from 550 K to 850 K (~35 to  
4 10 hPa) was the highest (i.e., most equatorward TrEL) June average observed throughout the 36-  
5 year period from 1979-2014. At 650 K the mean TrEL value at Lauder in June 2001 was ~31°S,  
6 indicating unusually tropical air relative to the latitude of the site.

7 From ~30 hPa to ~3 hPa,  $O_3$  generally increases from pole to equator throughout the year,  
8 hence the unusually high (equatorward) TrEL is associated with high  $O_3$ . We calculated the  
9 climatological monthly  $O_3$  latitudinal gradient from 45°S to 35°S from the MLS measurements,  
10 and found that from 20-10 hPa, this gradient peaks during the months of March-June. Hence  $O_3$   
11 mixing ratios measured over Lauder are particularly sensitive to changes in TrEL during these  
12 months. Thus the unusually high  $O_3$  anomaly in June 2001 is likely the result of an unusual  
13 amount of equatorward air over Lauder at a time when  $O_3$  variations are particularly sensitive to  
14 such transport.

15 To better explain the dynamics that caused this unusually high TrEL (and hence  $O_3$ ) over  
16 Lauder in June 2001 we show, in Fig. 4, the TrEL at 650 K (~20 hPa) for the entire Southern  
17 Hemisphere from 18 June – 2 July 2001. Low TrEL occurs throughout the polar vortex, also  
18 identified by streamlines (white contours) circling the pole. A strong anticyclone, identified by  
19 closed streamlines and elevated TrEL (marked with black “H”), moves eastward from 18-22  
20 June, before remaining relatively stationary for the next 8 days. This is an unusually strong  
21 “blocking” type pattern that kept high TrEL/high  $O_3$  air over Lauder. Figure 5 shows the vertical  
22 structure of this feature at 45°S, identified by zonal anomalies of geopotential height over a range  
23 of pressure surfaces from 1000 to 0.1 hPa. Elevated values extend from the tropopause (~200

1 hPa) into the lower mesosphere, tilting westward and narrowing with height. The anomaly peaks  
2 at  $\sim$ 10 hPa, with a longitudinal extent of  $\sim$ 120°. While this quasi-stationary stratospheric  
3 “Australian high” signature is known to occur in the SH spring (Harvey et al., 2002), this is the  
4 largest and most persistent episode observed in June in the 36-year TrEL simulation.

5

### 6 **3.2 Unusually high mid-stratospheric O<sub>3</sub> from August 2009 through July 2013**

7 The 4 years of elevated O<sub>3</sub> (2009-2013) occurred during the period when coincident Aura  
8 MLS measurements are available. Aura MLS overpasses occur near 01:15 and 14:30 local solar  
9 time at the latitude of Lauder. Since we are not using the MOPI1 measurements from 12:00-  
10 18:00, only the 01:15 overpasses are used. For comparison with MOPI1, we choose a longitude  
11 coincidence criterion of  $\pm$ 6°, which generally includes two daily 01:15 MLS overpasses. The  
12 monthly averages at 10 hPa from 2004-2014 are compared in Fig. 6. The MLS measurements  
13 show very good agreement with the MOPI measurements over the entire period, and both  
14 instruments show the large O<sub>3</sub> increase in mid-2009 and the large decrease in mid-2013. In mid-  
15 2009, mixing ratios increased from values near the lowest observed during the Lauder winter  
16 over this 10 year period, to values at, or near, the highest observed in a Lauder summer. There  
17 was a month-long gap in the MOPI1 measurements in July 2013, but the observed drop in the  
18 coincident MLS measurements is very similar to that of the MOPI1 measurements between June  
19 and August 2013. Both instruments show that, in August 2013, the O<sub>3</sub> values were the lowest  
20 since 2009.

21 The unusual nature of the 2009-2013 period is even more clearly emphasized in Fig. 7,  
22 which shows annual average anomalies from MOPI and from four satellite instruments that  
23 measured O<sub>3</sub> over extended periods since the early 1990’s. All of the measurements shown in

1 Fig. 7 are provided on their native grid. For the SAGE II measurements the native grid is  
2 altitude, and results are shown at 30 km. For HALOE, UARS and Aura MLS, and MOPI we  
3 show results at a 10 hPa. Note that, with the exception of the MOPI measurements, the  $O_3$   
4 anomalies shown in Fig. 7 are zonally averaged. Since only the MOPI1 measurements are  
5 available throughout the entire time period, all of the satellite measurements have been offset so  
6 that the average ozone matches that of MOPI1 during the period of coincidence. We note that  
7 there is an increase of ~4% in the MOPI measurements relative to both the locally coincident and  
8 the zonally averaged and convolved Aura MLS (shown in Fig. 6), which occurs primarily near  
9 the beginning of the Aura MLS timeseries. Since Fig. 7 shows annual averages it helps to  
10 emphasize the Quasi-Biennial Oscillation (QBO). The annual-average MOPI measurements  
11 show local minima in 1997, 1999, 2002, 2004, late 2006/early 2007, and late 2008/early 2009.  
12 Following the minimum in late 2008/early 2009 the  $O_3$  rises and remains well above the long-  
13 term average until 2013.

14

#### 15 **4. $O_3$ and $N_2O$ at Lauder and at the Equator**

##### 16 **4.1 Monthly $O_3$ anomaly correlations**

17 To better understand the global implications of the observed  $O_3$  variations over Lauder,  
18 we investigated how the variations in  $O_3$  observed over Lauder compare globally with changes in  
19 MLS  $O_3$ . We first calculated monthly averaged  $O_3$  at each MLS pressure level from 50 to 1 hPa  
20 in 2° latitude bins for 10 years of MLS data (2004-2014). We then calculated a climatological  
21 (i.e., 10-year) average for each calendar month. Using this climatology, we calculated an  
22 anomaly for each month of the 10-year series as a function of latitude and pressure. A similar  
23 monthly anomaly time series was calculated for the MOPI ozone at 10 hPa. Correlation

1 coefficients were calculated between the 10 hPa MOPI anomalies and the MLS anomalies at  
2 different pressures and latitudes, using months where both MLS and MOPI measurements were  
3 available.

4 Figure 8 shows the correlation coefficient ( $r$ ) as a function of pressure and latitude. The  
5 strongest correlation occurs slightly equatorward of Lauder and at a slightly higher pressure  
6 level. This is likely due to differences in instrumental errors, vertical resolution, and because the  
7 MOPI1 measurement is for local conditions near Lauder and not a zonal average. At the equator  
8 and 10 hPa there is a strong anti-correlation ( $r < -0.5$ ) between MOPI1 and MLS (the correlation  
9 between 10 hPa MLS  $O_3$  at  $45^\circ S$  and the equator is similar). There is also a weaker anti-  
10 correlation between MOPI1 and MLS  $O_3$  at  $\sim 20-45^\circ N$  below 10 hPa.

11 The geographical correlations seen in Fig. 8 are similar to those discovered by Randel  
12 and Wu (1996), who used singular value decomposition (SVD) analysis to study the relationship  
13 between QBO zonal winds and global SAGE  $O_3$  anomalies. The second mode of their analysis  
14 (SVD2; which explains 25% of the overall covariance) shows an anti-correlation between 10 hPa  
15  $O_3$  at Southern mid-latitudes and at the equator. It also shows a much weaker anti-correlation  
16 between 10 hPa  $O_3$  at Southern mid-latitudes and  $O_3$  at Northern mid-latitudes at slightly higher  
17 pressures.

18 Of course the temporal correlations shown in Fig. 8 give no indication of the time period  
19 over which the correlation is taking place (by using anomalies we have eliminated only the  
20 seasonal cycle), and could, e.g., represent QBO-like variations, solar cycle driven variations, or  
21 decadal-scale changes. What Fig. 8 certainly does emphasize is that the anomalies over Lauder  
22 at 10 hPa during the period 2004-2014 are not, predominantly, driven by a decadal scale global  
23 trend.

1

2 **4.2 Links between O<sub>3</sub> and N<sub>2</sub>O**

3 Nedoluha et al. (2015) showed that O<sub>3</sub> variations at the equator are very strongly  
4 positively correlated to variations in N<sub>2</sub>O. This relationship could best be understood as  
5 resulting from dynamical variations. Using a 2D chemical transport model, Nedoluha et al.  
6 (2015) showed that slower ascent resulted in more N<sub>2</sub>O being photodissociated and oxidized to  
7 produce NO<sub>x</sub> (while reducing N<sub>2</sub>O), and the increased NO<sub>x</sub> destroyed more ozone, resulting in a  
8 positive correlation between O<sub>3</sub> and N<sub>2</sub>O. Such a relationship has been previously deduced from  
9 changes in HALOE measurements of NO<sub>2</sub> at ~10 hPa from 1993-1997, where the change in NO<sub>2</sub>  
10 was shown to be consistent with a decrease in upward transport (Nedoluha et al., 1998).

11 In Fig. 9 we show monthly average anomalies for O<sub>3</sub> and N<sub>2</sub>O from Aura MLS and  
12 MOPI at 10 hPa. The variations in both O<sub>3</sub> and N<sub>2</sub>O from 5°S to 5°N (Fig. 9, right) show a clear,  
13 and similar, QBO signature. The connection between the QBO signal in O<sub>3</sub> and NO<sub>y</sub> (which is  
14 affected by N<sub>2</sub>O) was recognized in SAGE II data by Chipperfield et al. (1994), who pointed out  
15 that it was the result of QBO modulation of the vertical advection, with faster ascent resulting in  
16 larger O<sub>3</sub> mixing ratios in the mid-stratosphere.

17 In addition to O<sub>3</sub> and N<sub>2</sub>O, Fig. 9 shows the zonally averaged 30 hPa QBO winds over  
18 the equator from the Climate Data Assimilation System (from [www.cpc.ncep.noaa.gov](http://www.cpc.ncep.noaa.gov)). The 10  
19 hPa equatorial O<sub>3</sub> and N<sub>2</sub>O anomalies show a slight phase-lag relative to the 30 hPa QBO wind  
20 anomaly, but the generally positive correlation between this 30 hPa wind anomaly and O<sub>3</sub> and  
21 N<sub>2</sub>O mixing ratios suggests that an anomalously fast ascent rate near 10 hPa is associated with  
22 westerly (positive) winds at 30 hPa.

1       Figure 9 also shows that in 2006, 2008, 2010, and 2013 there are sharp increases in  $O_3$   
2       and  $N_2O$  from  $5^{\circ}S$  to  $5^{\circ}N$  near the middle of the year, while in 2007, 2009, and 2011 there are  
3       sharp decreases. Following these sharp changes the equatorial anomaly often remains high (or  
4       low) until the next June/July period. Thus the variation is often nearly biennial except for the  
5       absence of a change in sign for the  $O_3$  and  $N_2O$  anomalies from  $5^{\circ}S$  to  $5^{\circ}N$  in June/July 2012.

6       While the variation shown in Fig. 9 seems to be primarily nearly biennial, the period  
7       from 2009-2013 shows lower average equatorial  $O_3$  and  $N_2O$  mixing ratios than are observed  
8       from 2004-2008, as is apparent in the annual averages shown in Fig. 7. Figure 9 shows that the  
9        $5^{\circ}S$  to  $5^{\circ}N$   $O_3$  and  $N_2O$  mixing ratios have both lower maxima and lower minima at a similar  
10      phase of the QBO. While these equatorial  $N_2O$  and  $O_3$  anomalies are correlated with the phase  
11      of the QBO wind anomalies, it is not clear whether or not the unusually low  $O_3$  and  $N_2O$  mixing  
12      ratios in 2009-2013 are associated with unusual QBO wind anomalies.

13       There are some peculiarities in the QBO winds during the 2009-2013 period. For  
14      instance, the westerly wind anomalies in 2010 are weaker than the other four cycles during this  
15      period (16.0 m/s in August 2010 is the lowest maximum since 1992). The easterly 30 hPa wind  
16      anomalies in 2009/2010 are unusually strong for  $\sim 3$  months before an unusually fast transition  
17      back to westerly winds, while the 21.4 m/s maximum easterly wind anomaly in 2012 is the  
18      weakest over the four cycles shown. The 30 hPa wind anomalies during the 2008-2013 period  
19      persist for slightly longer than usual. The winds switched from easterly to westerly in March  
20      2008, August 2010, and March 2013, producing QBOs of length 29 months and 31 months  
21      respectively.

22       The 10 hPa  $O_3$  and  $N_2O$  anomalies at  $40^{\circ}S$  to  $50^{\circ}S$  (Fig. 9, left) are not as strongly  
23      correlated as at the equator (see Fig. 4, Nedoluha et al., 2015), but nonetheless there is clearly a

1 positive correlation between the anomalies of these two species. Not unexpectedly, given the  
2 correlations shown in Fig. 8, these Southern mid-latitude anomalies show variations that are  
3 usually opposite to those seen at the equator. Most clearly the sharp changes in June/July are  
4 anti-correlated with those near the equator. Figure 9 shows that, like the O<sub>3</sub> values that have  
5 been shown previously, the N<sub>2</sub>O values over latitudes near Lauder are elevated from 2009-2013.

6 The lower stratospheric anomalies in O<sub>3</sub> and N<sub>2</sub>O at 40°S to 50°S are likely to be caused  
7 by the variations in the rate at which tropical air with high N<sub>2</sub>O and low O<sub>3</sub> air moves into the  
8 Southern mid-latitudes, relative to the rate at which low N<sub>2</sub>O and high O<sub>3</sub> air descends into this  
9 region. The same tropical 30 hPa westerly winds which are associated with the increased ascent  
10 rate in the tropics seem to be correlated with a decrease in transport from the tropics into the  
11 Southern Hemisphere, resulting in an anti-correlation between N<sub>2</sub>O (and hence O<sub>3</sub>) anomalies at  
12 the tropics and the Southern mid-latitudes.

13

#### 14 **4.3 Decadal changes in O<sub>3</sub> and N<sub>2</sub>O**

15 To provide a global perspective on the 2009-2013 anomalies, we used linear regression to  
16 fit the MLS monthly mean data from August 2004 through May 2013 to 8 parameters, including  
17 annual and semi-annual sinusoidal terms, the 30 hPa and 50 hPa QBO winds, and a linear trend  
18 term. The linear trend terms from these fits are shown in Fig. 10. Based on the monthly MLS  
19 dataset that was used for the fit, the average 1- $\sigma$  uncertainty in the O<sub>3</sub> (N<sub>2</sub>O) trend fit is 0.008  
20 ppmv/yr (0.46 ppbv/yr), and it is <0.020 ppmv/yr (<1.05 ppbv/yr) everywhere in Fig. 10. The 1-  
21  $\sigma$  uncertainty in the O<sub>3</sub> (N<sub>2</sub>O) trend fit at 45°S is <0.011 ppmv/yr (<0.76 ppbv/yr). Since there is  
22 no clear correlation between the amplitude of the QBO wind variation and the depth of the N<sub>2</sub>O  
23 and O<sub>3</sub> changes in 2009-2013, these changes are fit by the linear trend term. The O<sub>3</sub> linear trend

1 fit plot (Fig. 10a) has been shown previously in Nedoluha et al. (2015), where it was shown that  
2 the decrease observed at 10 hPa near the equator has been occurring for more than 20 years.  
3 While a linear trend is clearly a very coarse representation of the MLS data from 2004-2013, it  
4 does allow us to show the strong global correlations between  $N_2O$  and  $O_3$  increases (and  
5 decreases) during this time period. While the beginning and ending dates are slightly different,  
6 Fig. 10 is qualitatively consistent with the conclusion in Mahieu et al. (2014) that the air in the  
7 SH mid-latitude lower stratosphere is younger in 2010/2011 than in 2005/2006, while the  
8 opposite is true in the NH.

9

## 10 **5. Discussion**

11 We have investigated two unusual  $O_3$  variations which occurred in the mid-stratosphere  
12 over Lauder, New Zealand during the 22 years of ground-based microwave measurements from  
13 the site. First, we examined a large positive  $O_3$  anomaly that was observed by the MOPI  
14 instrument in June 2001. The anomaly was associated with an unusually persistent stratospheric  
15 blocking anticyclone that kept air from more equatorial latitudes (with high ozone) over Lauder  
16 for much of this month. The very unusual nature of this event was emphasized by comparing the  
17 average Tracer Equivalent Latitude (TrEL) in June 2001 over Lauder on potential temperatures  
18 surfaces from 550 to 850 K (~35 to 10 hPa) with values found in other years. It was found that  
19 the TrEL in June 2001 was higher (i.e., more equatorward TrEL) than in any other June  
20 throughout the 36-year period 1979-2014.

21 The second interesting, and much longer-term, feature is the positive  $O_3$  anomaly near  
22 ~10 hPa which persists over Southern mid-latitudes from 2009-2013. During this period  $N_2O$  in  
23 this region is also unusually high, and the same chemical-dynamical relationship that causes the

1 very strong N<sub>2</sub>O-O<sub>3</sub> correlation in the tropics is likely the cause of the high O<sub>3</sub>. Briefly, N<sub>2</sub>O  
2 decreases rapidly both as a function of increasing altitude and increasing distance from the  
3 tropics due to photodissociation and oxidation. Thus the high N<sub>2</sub>O at Southern mid-latitudes  
4 from 2009-2013 suggests that air was transported into this region from the tropical lower  
5 stratosphere more quickly during this period, thus decreasing the amount of photodissociation  
6 and oxidation of N<sub>2</sub>O. At the same time, air was being transported more slowly into the tropical  
7 10 hPa region. The mid-2013 decrease in mid-latitude N<sub>2</sub>O suggests that air is now again being  
8 transported more quickly upwards in the tropics as opposed to being shifted towards Southern  
9 mid-latitudes, but it remains to be seen whether this is a brief interruption, a halt, or a reversal of  
10 a decadal scale trend.

11

12 **Acknowledgments.** We especially thank M. Kotkamp and A. Thomas for their long-term  
13 support of the MOPI instrument at Lauder. This project was funded by NASA under the Upper  
14 Atmosphere Research Program, by the Naval Research Laboratory, and by the Office of Naval  
15 Research. Work at the Jet Propulsion Laboratory, California Institute of Technology, was  
16 carried out under a contract with the National Aeronautics and Space Administration. MLS and  
17 HALOE data are available from the NASA Goddard Earth Science Data Information and  
18 Services Center (acdsc.gsfc.nasa.gov).

19

## 20 **References**

21 Allen, D. R., and Nakamura, N.: Tracer equivalent latitude: a diagnostic tool for isentropic  
22 transport studies, *J. Atmos. Sci.*, 60, 287-304, 2003.

1 Allen, D. R., Douglass, A. R., Nedoluha, G. E., and Coy, L.: Tracer transport during the Arctic  
2 stratospheric final warming based on a 33-year (1979-2011) tracer equivalent latitude  
3 simulation, *Geophys. Res. Lett.*, 39, L12801, doi:10.1029/2012GL051930, 2012.

4 Boyd, I. S., Parrish, A. D., Froidevaux, L., von Clarmann, T., Kyrola, E., Russell III, J. M., and  
5 Zawodny, J. M.: Ground-based microwave ozone radiometer measurements compared  
6 with Aura-MLS v2.2 and other instruments at two Network for Detection of Atmospheric  
7 Composition Change sites, *J. Geophys. Res.*, 112, D24S33, doi:10.1029/2007JD008720,  
8 2007.

9 Chipperfield, M. P., Gray, L. J., Kinnersley, J. S., and Zawodny, J.: A two-dimensional model  
10 study of the QBO signal in SAGE II NO<sub>2</sub> and O<sub>3</sub>, *Geophys. Res. Lett.*, 21, 589-592, 1994.

11 Connor, B. J., Parrish, A., Tsou, J. J., and McCormick, M. P.: Error analysis for the groundbased  
12 microwave ozone measurements during STOIC, *J. Geophys. Res.*, 100, 9283–9291, 1995.

13 Damadeo, R. P., Zawodny, J. M., Thomason, L. W., and Iyer, N.: SAGE version 7.0 algorithm:  
14 application to SAGE II, *Atmos. Meas. Tech.*, 6, 3539-3561, doi:10.5194/amt-6-3539-  
15 2013, 2013.

16 Eckert, E., von Clarmann, T., Kiefer, M., Stiller, G. P., Lossow, S., Glatthor, N., Degenstein, D.  
17 A., Froidevaux, L., Godin-Beekmann, S., Leblanc, T., McDermid, S., Pastel, M.,  
18 Steinbrecht, W., Swart, D. P. J., Walker, K. A., and Bernath, P. F.: Drift-corrected trends  
19 and periodic variations in MIPAS IMK/IAA ozone measurements, *Atmos. Chem. Phys.*,  
20 14, 2571–2589, doi:10.5194/acp-14-2571-2014, 2014.

21 Froidevaux, L., Read, W. G., Lungu, T. A., Cofield, R. E., Fishbein, E. F., Flower, D. A., Jarnot,  
22 R. F., Ridenoure, B. P., Shippoly, Z. , Waters, J. W., Margitan, J. J., McDermid, I. S.,  
23 Stachnik, R. A., Peckham, G. E., Braathen, G., Deshler, T., Fishman, J., Holmann, D. J.,

1 and Oltmans, S. J.:Validation of UARS Microwave Limb Sounder Ozone Measurements,  
2 J. Geophys. Res., 101, D6, 10017–10060, 1996.

3 Froidevaux, L., Jiang, Y. B., Lambert, A., Livesey, N. J., Read, W. G., Waters, J. W., Browell,  
4 E. V., Hair, J. W., Avery, M. A., McGee, T. J., Twigg, L. W., Sumnicht, G. K., Jucks, K.  
5 W., Margitan, J. J., Sen, B., Stachnik, R. A., Toon, G. C., Bernath, P. F., Boone, C. D.,  
6 Walker, K. A., Filipiak, M. J., Harwood, R. S., Fuller, R. A., Manney, G. L., Schwartz,  
7 M. J., Daffer, W. H., Drouin, B. J., Cofield, R. E., Cuddy, D. T., Jarnot, R. F., Knosp, B.  
8 W., Perun, V. S., Snyder, W. V., Stek, P. C., Thurstans, R. P., and Wagner, P. A.:  
9 Validation of Aura Microwave Limb Sounder stratospheric ozone measurements, J.  
10 Geophys. Res., 113, D15S20, doi:10.1029/2007JD008771, 2008.

11 Gebhardt, C., Rozanov, A., Hommel, R., Weber, M., Bovensmann, H., Burrows, J. P.,  
12 Degenstein, D., Froidevaux, L., and Thompson, A. M.: Stratospheric ozone trends and  
13 variability as seen by SCIAMACHY from 2002 to 2012, Atmos. Chem. Phys., 14, 831–  
14 846, doi:10.5194/acp-14-831-2014, 2014.

15 Harvey, V. L., Pierce, R. B., Fairlie, T. D., and Hitchman, M. H.: A climatology of stratospheric  
16 polar vortices and anticyclones, J. Geophys. Res., 107, 4444,  
17 doi:10.1029/2001JD001471, 2002

18 Kyrölä, E., Laine, M., Sofieva, V., Tamminen, J., Päivärinta, S.-M., Tukiainen, S., Zawodny, J.,  
19 and Thomason, L.: Combined SAGE II–GOMOS ozone profile data set for 1984–2011  
20 and trend analysis of the vertical distribution of ozone, Atmos. Chem. Phys., 13, 10645–  
21 10658, doi:10.5194/acp-13-10645-2013, 2013.

22 Lambert, A., Read, W. G., Livesey, N. J., Santee, M. L., Manney, G. L., Froidevaux, L., Wu, D.,  
23 Schwartz, M. J., Pumphrey, H. C., Jimenez, C., Nedoluha, G. E., Cofield, R. E.,

1 Cuddy, D. T., Daffer, W. H., Drouin, B. J., Fuller, R. A., Jarnot, R. F., Knosp, B. W.,  
2 Pickett, H. M., Perun, V. S., Snyder, W. V., Stek, P. C., Thurstans, R. P., Wagner, P. A.,  
3 Waters, J. W., Jucks, K. W., Toon, G. C., Stachnik, R. A., Bernath, P. F., Boone, C. D.,  
4 Walker, K. A., Urban, J., Murtagh, D., Elkins, J. W., and Atlas, E.: Validation of the  
5 Aura Microwave Limb Sounder middle atmosphere water vapor and nitrous oxide  
6 measurements, *J. Geophys. Res.*, 112, D24S36, doi:10.1029/2007JD008724, 2007.

7 Livesey, N. J., Read, W. G., Froidevaux, L., Waters, J. W., Santee, M. L., Pumphrey, H. C., Wu,  
8 D. L., Shippony, Z., and Jarnot, R. F.: The UARS Microwave Limb Sounder version 5  
9 data set: theory, characterization, and validation, *J. Geophys. Res.*, 108, 4378,  
10 doi:10.1029/2002JD002273, 2003.

11 Mahieu, E., Chipperfield, M. P., Notholt, J., Reddmann, T., Anderson, J., Bernath, P. F.,  
12 Blumenstock, T., Coffey, M. T., Dhomse, S. S., Feng, W., Franco, B., Froidevaux, L.,  
13 Griffith, D. W. T., Hannigan, J. W., Hase, F., Hossaini, R., Jones, N. B., Morino, I.,  
14 Murata, I., Nakajima, H., Palm, M., Paton-Walsh, C., Russell, J. M., Schneider, M.,  
15 Servais, C., Smale, D., Walker, K. A.: Recent Northern Hemisphere stratospheric HCl  
16 increase due to atmospheric circulation changes, *Nature*, doi:10.1038/nature13857, 2014.

17 Nazaryan, H., McCormick, M. P., and Russell III, J. M.: New studies of SAGE II and HALOE  
18 ozone profile and long-term change comparisons, *J. Geophys. Res.*, 110, D09305,  
19 doi:10.1029/2004JD005425, 2005.

20 Nedoluha, G. E., Siskind, D. E., Bacmeister, J. T., Bevilacqua, R. M., and Russell III, J. M.:  
21 Changes in upper stratospheric CH<sub>4</sub> and NO<sub>2</sub> as measured by HALOE and implications  
22 for changes in transport, *Geophys. Res. Lett.*, 25, 987–990, 1998.

1 Nedoluha, G. E., Siskind, D. E., Lambert, A., and Boone, C.: The decrease in mid-stratospheric  
2 tropical ozone since 1991, *Atmos. Chem. Phys. Discuss.*, 453–480, doi:10.5194/acpd-15-  
3 453-2015, 2015.

4 Randel, W. J., and Wu, F.: Isolation of the ozone QBO in SAGE II data by singular-value  
5 decomposition, *J. Atmos. Sci.*, 53, 2546-2559, 1996.

6 Parrish, A.: Millimeter-wave remote sensing of ozone and trace constituents in the stratosphere,  
7 P. IEEE, 82, 1915–1929, 1994.

8 Parrish, A., deZafra, R. L., Solomon, P. M., and Barrett, J. W.: A ground-based technique for  
9 millimeter wave spectroscopic observations of stratospheric trace constituents, *Radio*  
10 *Sci.*, 23, 106-118, 1988.

11 Parrish, A., Connor, B. J., Tsou, J. J., McDermid, I. S., and Chu, W. P.: Ground-based  
12 microwave monitoring of stratospheric ozone, *J. Geophys. Res.*, 97, 2541–2546, 1992.

13 Parrish, A., Boyd, I. S., Nedoluha, G. E., Bhartia, P. K., Frith, S. M., Kramarova, N. A., Connor,  
14 Bodeker, G. E., Froidevaux, L., Shiotani, M., and Sakazaki, T.: Diurnal variations  
15 of stratospheric ozone measured by ground-based microwave remote sensing at the  
16 Mauna Loa NDACC site: measurement validation and GEOSCCM model comparison,  
17 *Atmos. Chem. Phys.*, 14, 7255–7272, doi:10.5194/acp-14-7255-2014, 2014.

18 Rodgers, C. D., Retrieval of atmospheric temperature and composition from remote  
19 measurements of thermal radiation, *Rev. Geophys.*, 14, 609–624, 1976.

20 Steinbrecht, W., Claude, H., Schönenborn, F., McDermid, I. S., Leblanc, T., Godin-Beekmann,  
21 S., Keckhut, P., Hauchecorne, A., Van Gijsel, J. A. E., Swart, D. P. J., Bodeker, G. E.,  
22 Parrish, A., Boyd, I. S., Kämpfer, N., Hocke, K., Stolarski, R. S., Frith, S. M., Thomason,  
23 L. W., Remsberg, E. E., Von Savigny, C., Rozanov, A., and Burrows, J. P.: Ozone and

1 temperature trends in the upper stratosphere at five stations of the Network for the  
2 Detection of Atmospheric Composition Change, *Int. J. Remote Sens.*, 30, 3875–3886,  
3 doi:10.1080/01431160902821841, 2009.

4 Wang, H. J., Cunnold, D. M., Thomason, L. W., Zawodny, J. M., and Bodeker, G. E.:  
5 Assessment of SAGE version 6.1 ozone data quality, *J. Geophys. Res.*, 107, 4691,  
6 doi:10.1029/2002JD002418, 2002.

7 WMO Global Ozone Research and Monitoring Project Report No. 54: Report of the Ninth  
8 Meeting of the Ozone Research Managers of the Parties to the Vienna Convention for the  
9 Protection of the Ozone Layer, Geneva, Switzerland, 14-16 May 2014, 2014.

10

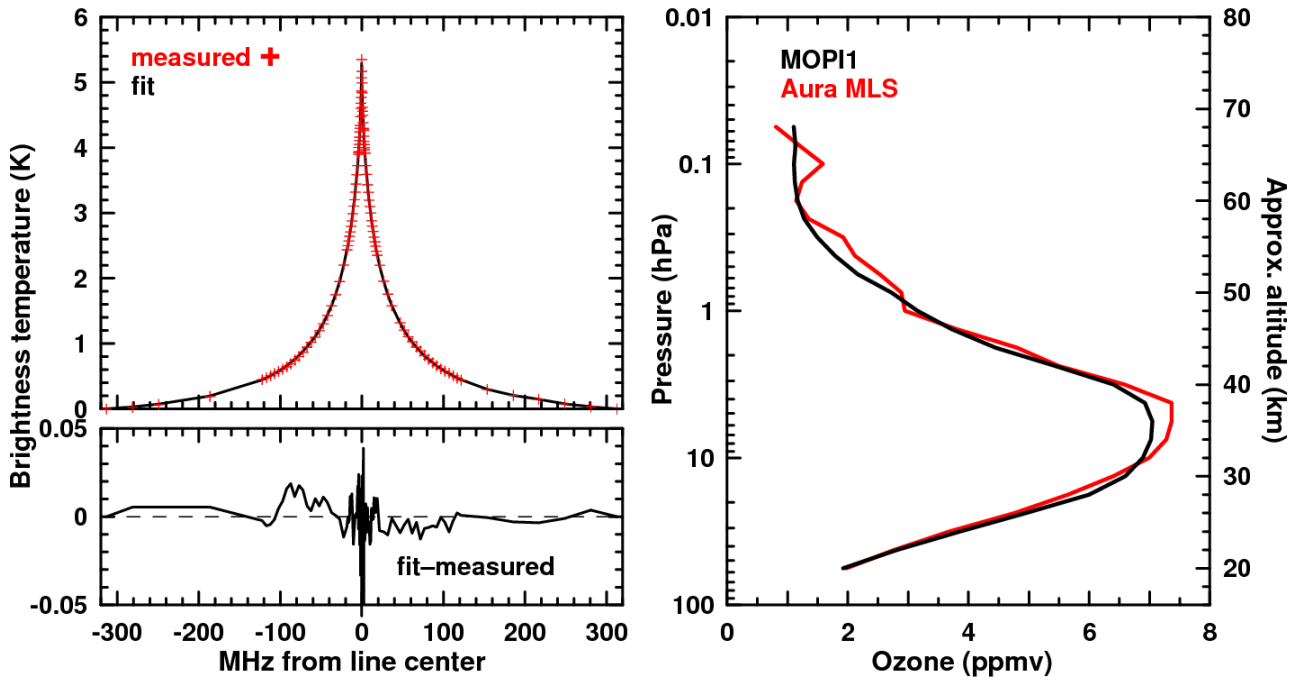
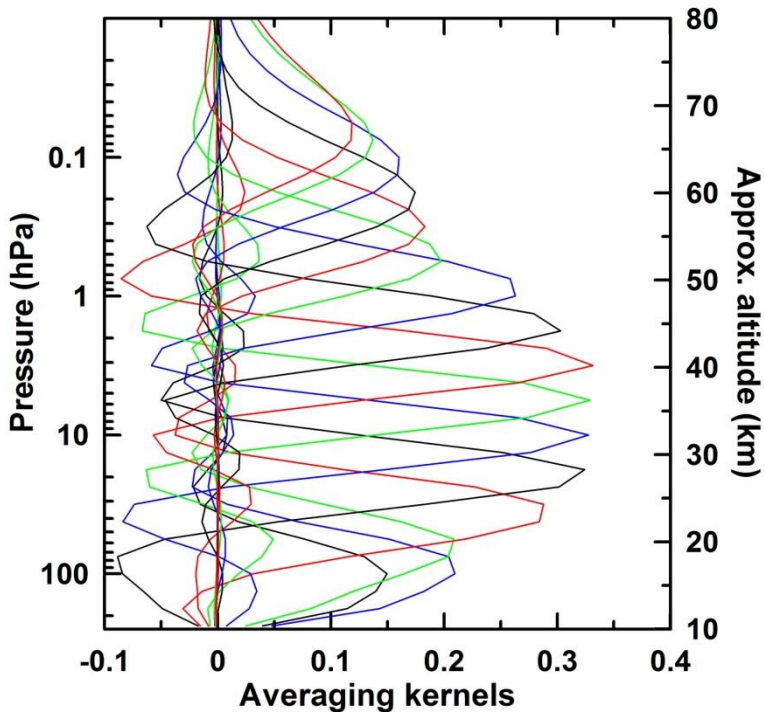
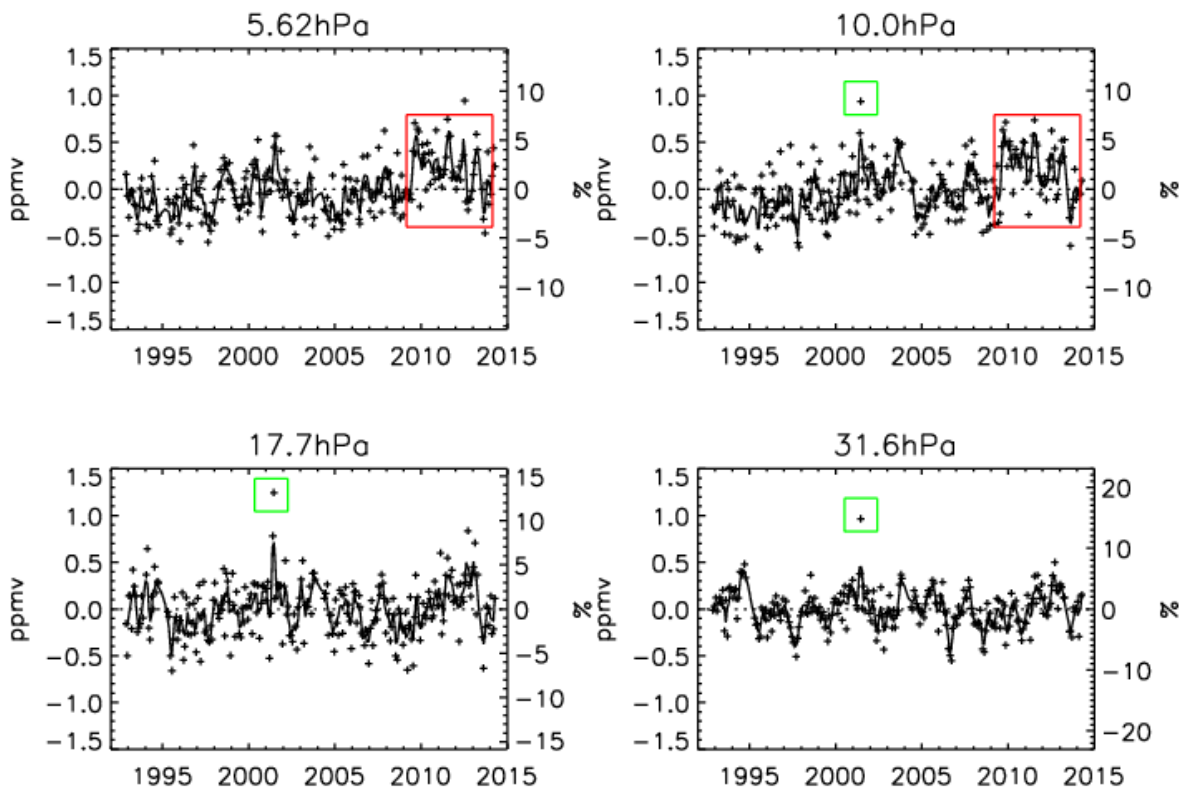


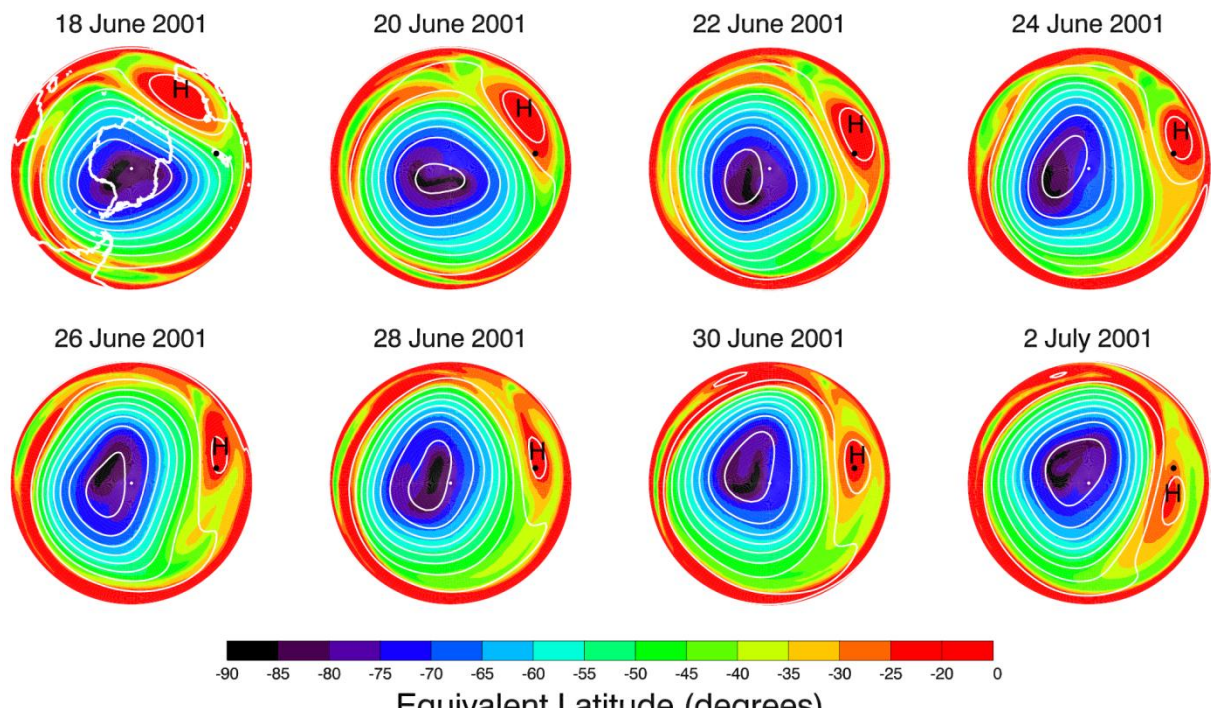
Figure 1 – Top left: The spectrum centered at 110.836GHz as measured by MOPI1 from Lauder over 3 h on 11 March 2014 (red crosses), and the model fit to this spectrum (black line). Bottom left: The residual difference between the measured and modeled spectrum. Right: The retrieved  $O_3$  profile from MOPI1 (black) and from a coincident Aura MLS measurement (red).



1  
2 Figure 2 – Typical averaging kernels for the MOPI1 instrument based on 6 h of spectral integration. Averaging kernels are  
3 shown for every second level, with the averaging kernels in blue shown at 100, 10, 1, and 0.1 hPa.



4  
5 Figure 3 – Crosses show monthly ozone anomalies from the MOPI1 measurements. The line shows a 3-point smoothing of  
6 the data. Boxes indicate periods of particular interest (see text).



4

5 Figure 4 – The tracer equivalent latitude (see text) for the Southern Hemisphere at 650 K. The location of Lauder ( $45^{\circ}\text{S}$ ,  

6  $169.7^{\circ}\text{E}$ ) is indicated by a black dot. White contours are 650 K streamlines at constant intervals. The black “H” indicates the  

7 location of strong anticyclonic circulation.

8

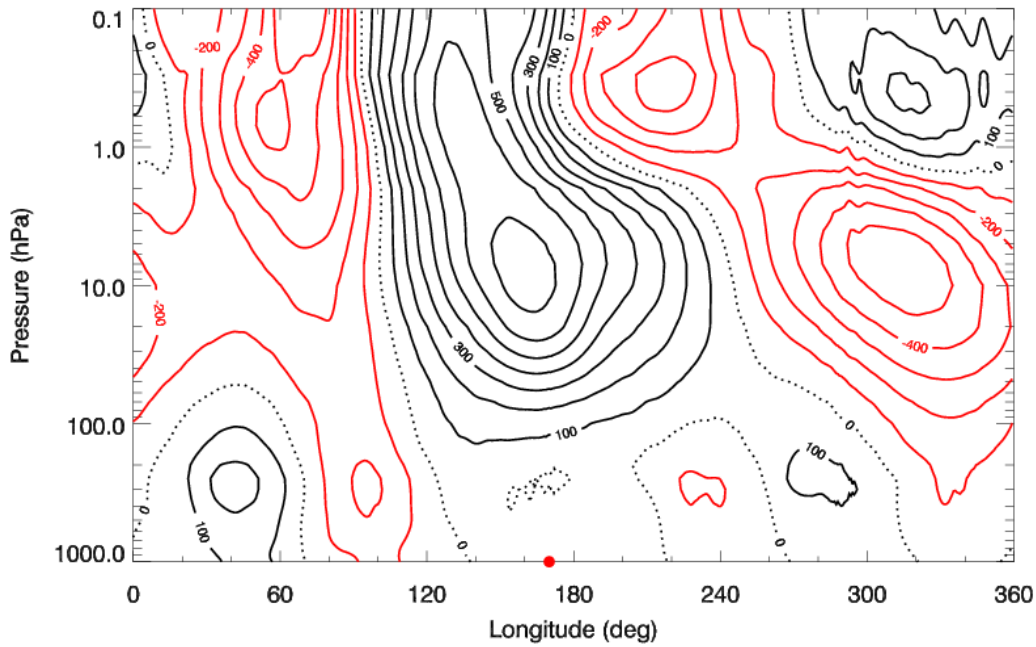


Figure 5 - The MERRA geopotential height anomaly, in 100 m increments, calculated for the period 21-30 June 2001, at 45°S. The longitude of Lauder is indicated by the red dot. Positive (negative) anomalies are identified by solid black (red) contours, while the black dotted line indicates zero anomaly.

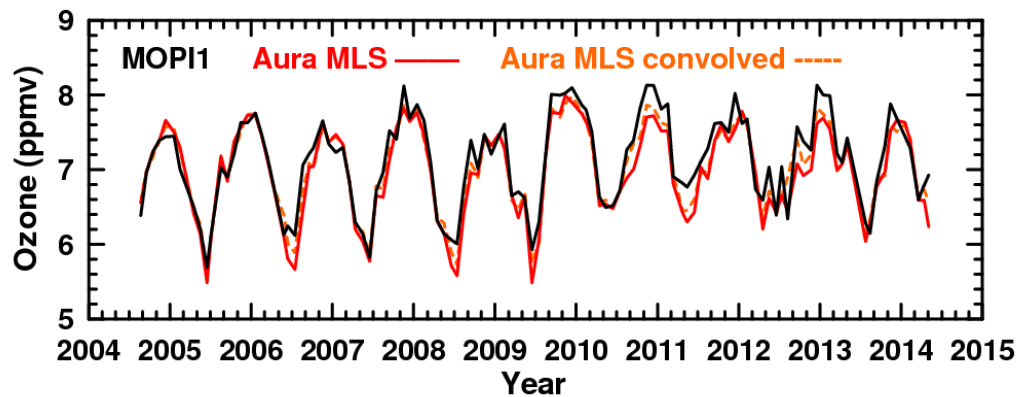


Figure 6 - Monthly ozone averages for MOPI1 (black), Aura MLS (red), and Aura MLS convolved with the MOPI averaging kernels (dashed orange) measurement pairs at 10 hPa. Measurements are shown when there is an MLS measurement taken within  $\pm 1^\circ$  latitude and  $\pm 6^\circ$  longitude within 6 hours of a MOPI measurement.

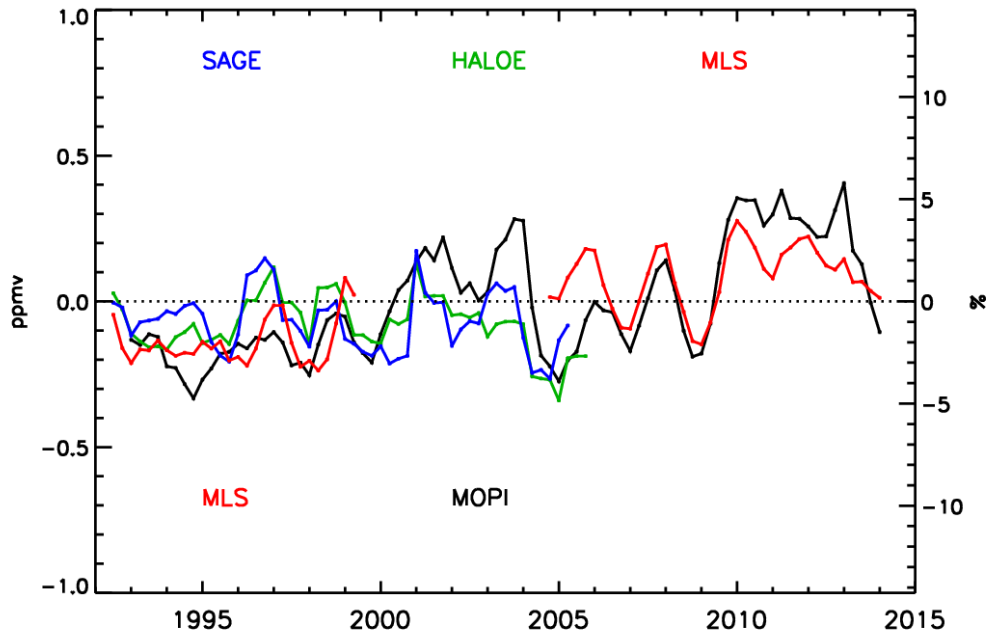


Figure 7 Annual average ozone anomalies at 10 hPa (30 km for SAGE II) shown 4-times annually (with annual averages taken from January-December, April-March, July-June, and October-September). Results are shown for SAGE II (blue), HALOE (green), UARS and Aura MLS (both red), and MOPI1 (black). Satellite measurements (latitudinal averages from 40°S-50°S) have been offset so that the average ozone matches that of MOPI1 during the period of coincidence.

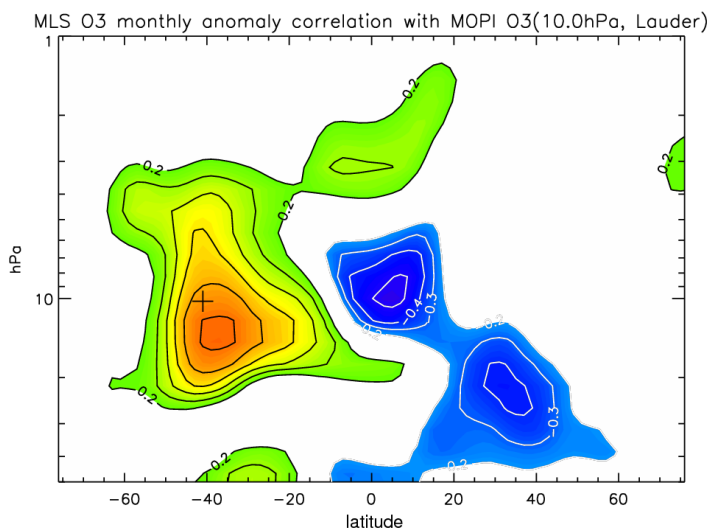
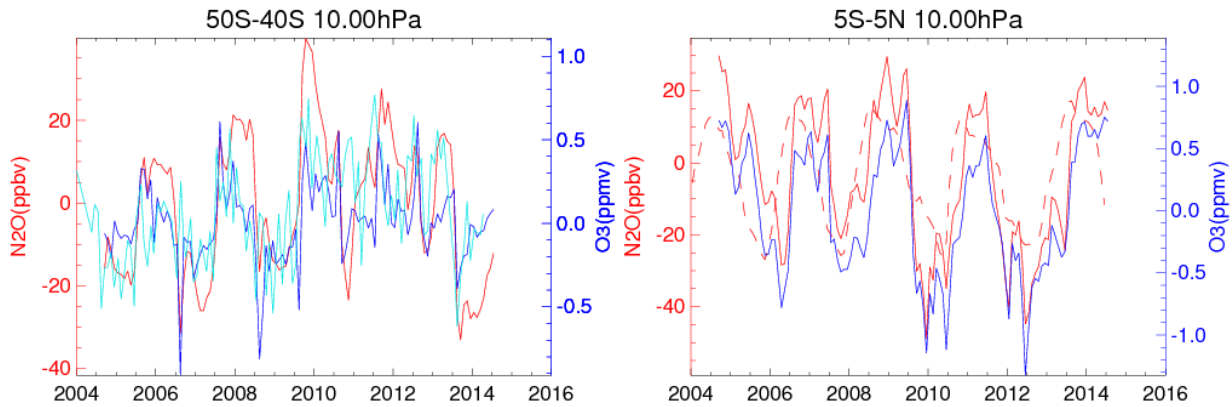


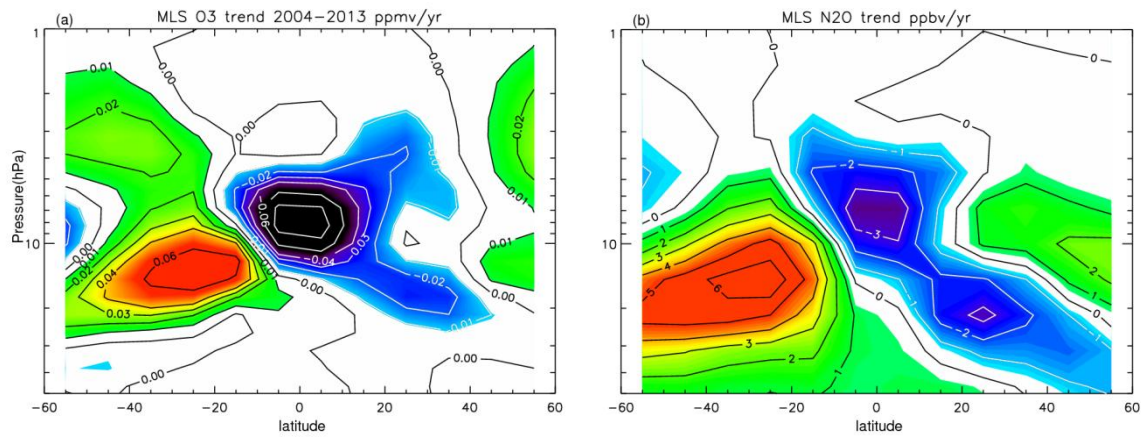
Figure 8 - The correlation coefficient of the monthly MLS O<sub>3</sub> anomalies with the monthly anomalies of the MOPI1 O<sub>3</sub> measurements at 10 hPa. The cross represents the latitude of Lauder at 10 hPa.

1  
2



3  
4 **Figure 9** - Monthly average anomalies for N<sub>2</sub>O (red) and O<sub>3</sub> (blue) as measured by MLS at 10 hPa within 5° of the Lauder  
5 latitude (45°S) (left) and within 5° of the equator (right). The left hand plot also shows the monthly average O<sub>3</sub> anomalies  
6 (based on the 2004–2014 averages) for MOPI (cyan). The right hand plot also shows (dashed red line) the 30 hPa QBO index  
7 in m s<sup>-1</sup>, using the same numerical scale as the N<sub>2</sub>O in ppbv.

8  
9  
10  
11  
12  
13



14  
15 **Figure 10** - Linear trend fits to MLS O<sub>3</sub> and N<sub>2</sub>O measurements from August 2004 through May 2013. Contour lines for O<sub>3</sub> are  
16 shown at +/-0.01, 0.02, 0.03, 0.04, 0.06, 0.08 ppmv yr<sup>-1</sup>. Contour lines for N<sub>2</sub>O are shown at intervals of 1 ppmv yr<sup>-1</sup>. The O<sub>3</sub>  
17 figure is from Nedoluha et al. (2015).

18